A new 1D Zn(II) coordination polymer containing 2-amino-4,6-dimethoxypyrimidine ligand: crystal structure, Hirshfeld surface analysis, and physicochemical studies

Rim Boubakri, Christian Jelsch, Christine Lucas, Frédéric Lefebvre, Werner Kaminsky, Cherif Ben Nasr, Kamel Kaabi

Published in *Journal of Molecular Structure*, 2020 , 128309.

doi.org/10.1016/j.molstruc.2020.128309

A new 1D Zn(II) coordination polymer containing 2-amino-4,6-dimethoxypyrimidine ligand: crystal structure, Hirshfeld surface analysis, and physicochemical studies

Rim Boubakri[1], Christian Jelsch[2], Christine Lucas[3], Frédéric Lefebvre[3], Werner Kaminsky[4], Cherif Ben Nasr[1], Kamel Kaabi[1]*

[1] Laboratoire de Chimie des Matériaux, Université de Carthage, Faculté des Sciences de Bizerte, 7021 Zarzouna, Tunisie.

[2] CRM[2], CNRS, Institut Jean Barriol, Université de Lorraine, 54000 Nancy, France.

[3] Laboratoire de Chimie Organométallique de Surface (LCOMS), Ecole Supérieure de Chimie Physique Electronique, 69626 Villeurbanne Cedex, France.

[4] Department of Chemistry, BOX 351700 University of Washington Seattle, WA 98195, USA.

*Corresponding e-mail: kamel_kaabi@yahoo.fr

Abstract

A new 1-D polymeric zinc(II) complex derived from the neutral bidentate 2-amino-4,6-dimethoxypyrimidine ligand of formula $[Zn_2Cl_4(C_6H_9N_3O_2)_2]_n$ has been prepared and characterized by single crystal X-ray diffraction, elemental analysis and IR spectroscopy. The Zn(II) cations are tetra-coordinated, in a tetrahedral fashion, by two nitrogen atoms from the pyrimidine ring of the organic ligand and two chloride anions. In the atomic arrangement, the bridge bidentate 2-amino-4,6-dimethoxypyrimidine ligands and the tetra-connected Zn centers link each other to give a 1-D corrugated chain with molecular formula $[Zn_2Cl_4(C_6H9N_3O_2)_2]_n$ running along the *b*-axis direction. These chains, located at $z = (2n+1)/4$, are interconnected via C-H···Cl^- hydrogen bonds to form layers parallel to the (**a**, **c**) plane and crossing the unit cell at $y = ½$. These layers are, in turn, connected to each other via C-H···Cl^- hydrogen bonds to form a three-dimensional supramolecular network. Intermolecular interactions were investigated by Hirshfeld surfaces. The two independent organic ligands show very similar contacts and electrostatic environments. Electronic properties such as HOMO and LUMO energies were derived. The vibrational absorption bands were identified by infrared spectroscopy. This compound was also characterized by thermal analysis to determine its thermal behavior.

Keywords: Zn(II) complex, X-ray diffraction, Hirshfeld surface, CP-MAS-NMR spectroscopy, Hydrogen bonds.

1. Introduction

Recently, metal-organic complexes have gained more interest due to their potential applications in several fields such as material [1] and medicinal chemistry [2], not only because of their great interesting structural diversity, but also due to their extensive exploitable properties such as in gas or liquid adsorption, ion exchange, catalysis, separation, magnetism, sensing [3–8], radio-immunotherapy and magnetic resonance imaging [9, 10]. Among these complexes, the Zn complexes have interesting physical properties especially their photoluminescence allowing them to be used as sensors, biological imaging probes and electrochemical devices [11-17]. Furthermore, the external electronic configuration d^{10} of Zn (II) gives a stabilization energy of the zero crystal field which allows this cation to adopt various geometries, in particular the

tetrahedron, the octahedron and the dodecahedron [18]. As part of our continued involvement in the investigation of metal complexes, we report here the synthesis and characterization of a new Zn(II) complex with the 4-amino-6-methoxypyrimidine ligand. We chose a pyrimidine derivative as an organic ligand because the resulting complexes show interesting structural, chemical, and physical properties significant for photoluminescence, magnetism, ferroelectricity, conductivity, and non-linear optics [9–12]. The Hirshfeld surface analysis was performed to completely characterize the intermolecular interactions and explain the crystalline architecture. Moreover, the vibrational characteristics and NMR properties were also studied and DFT calculations were used for the interpretation of the results.

2. Materials and methods

2.1. Chemical preparation

A solution of $ZnCl_2$ (54.52 mg, 0.4 mmol, Sigma-Aldrich) in water (10 mL) was added drop wise to a solution of 2-amino-4,6-dimethoxypyrimidine (62.1 mg, 0.4 mmol, Sigma-Aldrich) in ethanol (10 mL). After stirring for 45 min, the mixture was filtered and the resultant solution was allowed to evaporate at room temperature. Transparent prismatic single crystals of the title compound, which remained stable under normal conditions of temperature and humidity, were isolated after several days and subjected to X-ray diffraction analysis (yield 68%). Anal. Calc. for $[Zn_2Cl_4(C_6H_9N_3O_2)_2]$: C, 24.71 %; H, 3.08 %; N, 14.41 %. Found: C, 24.92 %; H, 3.51 %; N, 14.78 %.

2.2. Investigation techniques

2.2.1. X-ray data collection and structure solution

A colorless prism, measuring 0.13 x 0.12 x 0.09 mm^3 was mounted on a loop with oil. Data were collected at 21ºC on a Nonius Kappa CCD FR590 single crystal X-ray diffractometer using the Mo-radiation. Crystal-to-detector distance was 30 mm and exposure time was 90 seconds per degree for all sets. The scan width was 1.5º. Data collection was 99.5% complete to 25º in θ. 9529 merged reflections were collected covering the indices, $-10 \leq h \leq 10$, $-22 \leq k \leq 25$, $-19 \leq l \leq 19$. 5366 reflections were symmetry independent and the $R_{int} = 0.0437$ factor indicated that the diffraction data were of good quality. Indexing and unit cell refinement indicated the

monoclinic lattice. The space group was found to be $P2_1/n$ (N°. 14). The data were integrated and scaled using hkl-SCALEPACK [23]. This program applies a multiplicative correction factor (*S*) to the observed intensities (*I*) and has the following form:

$$S = (e^{-2B(\sin^2\theta)/\lambda^2}) / \text{scale}$$

S is calculated from the scale factor and the *B* factor which are determined for each frame and is then applied to *I* to give the corrected intensity (I_{corr}).

Solution by direct methods (SHELXS, SIR97 [24]) produced a complete heavy atom phasing model consistent with the proposed structure. The structure was completed by difference Fourier synthesis with SHELXL97 [25-26]. Scattering factors were from Waasmair and Kirfel [27]. Hydrogen atoms were placed in geometrically idealized positions and constrained to ride on their parent atoms with C---H distances in the range 0.95-1.00 Å. Isotropic thermal parameters U_{iso} were fixed such that they were $1.2U_{eq}$ of their parent atom for CH and NH_2 groups and $1.5U_{eq}$ of their parent atom for methyl groups. All non-hydrogen atoms were refined anisotropically by full-matrix least-squares. The drawings were made with Diamond [28]. Crystal data and experimental parameters used for the intensity data collection are summarized in Table 1.

Table 1 Experimental details of coordination polymer $[Zn_2Cl_4(C_6H_9N_3O_2)_2]_n$

Crystal data	
Chemical formula	$C_{12}H_{18}Cl_4N_6O_4Zn_2$
M_r (g.mol^{-1})	582.86
D_x (Mg m^{-3})	1.757
F(000)	1168
Crystal system, space group	Monoclinic, $P2_1/n$
Temperature (K)	294
a, b, c (Å)	7.5855 (3), 19.7127 (9), 14.8326 (6)
β (°)	96.599 (2)
V (Å^3)	2203.23 (16)
Z	4
Radiation type	Mo$K\alpha$ (λ = 0.71073 Å)
μ (mm^{-1})	2.69
Crystal size (mm)	0.13 × 0.12 × 0.09
Data collection	
Diffractometer	KappaCCD
No. of measured, independent and observed [$I > 2\sigma(I)$] reflections	9529, 5366, 3165
R_{int}	0.047
$\sin\theta_{max}/\lambda$ (Å^{-1})	0.667
Refinement	
$R[F^2 > 2\sigma(F^2)]$, $wR(F^2)$, S	0.041, 0.087, 0.96
No. of reflections	5366
No. of parameters	257
H-atom treatment	H-atom parameters constrained
$\Delta\rho_{max}$, $\Delta\rho_{min}$ (e Å^{-3})	0.38, −0.55

2.2.4. Infrared spectroscopy

The Fourier Transform Infrared (FTIR) spectrum of a powder sample was obtained using a Nicolet 5700 spectrophotometer with potassium bromide (KBr) pellets (2 mg of sample in 200 mg of KBr). The number of scans was 32. The scanning range was 4000–400 cm^{-1} and the resolution 2 cm^{-1}.

2.2.5. DFT calculations

DFT calculations were performed with the Gaussian 09 Revision A-02 software [29]. The B3LYP functional was used with the 6-31+G* base set for all atoms, including zinc. Two studies were made, one on a species containing one $ZnCl_2$ group and the two organic ligands and one where the effect of the two surrounding $ZnCl_2$ groups was included, the coordination of Zn being completed by a NH_3 group. The positions of all non-hydrogen atoms were those determined by the X-ray diffraction study. The positions of hydrogens were optimized at the B3LYP/6-31+G* level, starting from the positions of the X-ray diffraction study. The spectroscopic parameters (NMR and infrared spectra) were then calculated on this semi-optimized geometry.

3. Results and discussion

3.1. Structure description

The main geometrical features of zinc(II) coordination polymer of formula $[Zn_2Cl_4(C_6H_9N_3O_2)_2]_n$ are reported in Tables 2 and 3. The zinc polymeric complex crystallizes in the monoclinic space group $P2_1/n$. The asymmetric unit of the title compound consists of two Zn(II) cations, two neutral bidentate 2-amino-4,6-dimethoxypyrimidine ligands and four chloride ions Cl^- (**Fig. 1)**. The asymmetric unit is in fact a $[Zn_2Cl_4(C_6H_9N_3O_2)_2]$ unit which leads to a 1-D chain with molecular formula $[Zn_2Cl_4(C_6H_9N_3O_2)_2]_n$ running along the *b*-axis direction (**Fig. 2**). The coordination geometry around each Zn(II) atom can be described as a distorted tetrahedral $ZnCl_2N_2$ moiety. Each Zn(II) center is tetracoordinated by two nitrogen from the pyrimidine ring of the organic ligand and two chloride anions (N1, N4, Cl1 and Cl2 for Zn(1); N2, N5, Cl3 and Cl4 for Zn(2)). In the atomic arrangement of this compound, the Zn-N and Zn-Cl bond lengths vary respectively in the range 2.082(3)-2.2401(9) and 2.077(3)-2.2381(10) Å and the bond angles around the Zn atom vary between 97.24(10) and 115.30(8)° for the $Zn(1)Cl_2N_2$ tetrahedron and between 107.96(9) and 112.02(4)° for the $Zn(2)Cl_2N_2$

tetrahedron (Table 2). These values are similar to those reported for other tetrahedral Zn(II) complexes such as 2-[(2-aminoethyl)amino]ethanaminium dichlorozincate [30] and 4-(3,5-diphenyl-1H-pyrazol-1-yl)-6-(piperidin-1-yl)pyrimidine dichlorozincate complexes [31]. The geometry of four-coordinated metal complex my conveniently be measured by the Yang τ_4-parameter [32], $\tau_4 = [360 - (\beta + \alpha)]/141$ with β and α being the two largest angles, that is zero for a perfect square planar geometry and one for a perfect tetrahedral geometry.

Table 2 Selected bond distances and angles (Å, º) in the title complex

N1—Zn1	2.092 (3)	N4—Zn1—N1	97.24 (10)
N4—Zn1	2.082 (3)	N4—Zn1—Cl1	115.30 (8)
Cl1—Zn1	2.2152 (10)	N1—Zn1—Cl1	112.74 (8)
Cl2—Zn1	2.2401 (9)	N4—Zn1—Cl2	113.07 (8)
N2—Zn2	2.084 (2)	N1—Zn1—Cl2	110.28 (8)
N5—Zn2^{i}	2.077 (3)	Cl1—Zn1—Cl2	107.95 (4)
Cl3—Zn2	2.2471 (10)	N5^{ii}—Zn2—N2	111.02 (10)
Cl4—Zn2	2.2381 (10)	N5^{ii}—Zn2—Cl4	107.96 (9)
C1—N1	1.347 (4)	N2—Zn2—Cl4	111.89 (8)
C1—C2	1.375 (4)	N5^{ii}—Zn2—Cl3	109.06 (8)
C2—C3	1.371 (4)	N2—Zn2—Cl3	104.88 (8)
C3—N2	1.343 (4)	Cl4—Zn2—Cl3	112.02 (4)
C4—N3	1.327 (4)	C10—N6	1.336 (4)
C4—N2	1.344 (4)	C10—N4	1.342 (4)
C4—N1	1.353 (4)	C10—N5	1.351 (4)
C9—N4	1.344 (4)	C7—O3	1.330 (4)
C1—O1	1.328 (4)	C11—O3	1.442 (4)
C5—O1	1.430 (4)	C9—O4	1.324 (4)
C3—O2	1.339 (4)	C12—O4	1.449 (4)
C6—O2	1.443 (4)		

Symmetry codes: (i) $-x-½, y+½, -z+½$; (ii) $-x-½, y-½, -z+½$.

The calculated τ_4 values of the title compound areτ_4(Zn1) = 0.93 for the Zn(1)Cl_2N_2 tetrahedron (β = 115.30 (8)° and α = 113.07 (8)°) and τ_4(Zn2) = 0.96 for the Zn(2)Cl_2N_2 tetrahedron (β = 112.02 (4)° and α = 111.89 (8)°), indicating a quite small distortion from the regular tetrahedral and that the first tetrahedron is slightly more distorted than the second one. The chains $[Zn_2Cl_4(C_6H_9N_3O_2)_2]_n$, located at $z = (2n+1)/4$, are interconnected via C12—H···Cl1 (C…Cl = 3.776 (4) Å) and C5—H···Cl2 (C…Cl = 3.542 (3) Å) weak hydrogen bonds (Table 3) to form layers parallel to the (**a**, **c**) plane which cross the unit cell at $y = ½$ (**Figs. 3 and 4**). These layers are; in turn, connected to each other via C6—H···Cl2, C8—H···Cl3 and C11—H···Cl3 hydrogen bonds to form a three-dimensional supramolecular network (Fig. 4). Moreover, the cohesion of the structure of this compound is reinforced by strong hydrogen bonds of type N—H…Cl whose N...Cl distances vary between 3.184 (3) and 3.268 (3) Å.

Table 3. Hydrogen-bond geometry (Å, º) in the title complex.

D*—H···*A	***D*—H**	**H···*A***	***D*···*A***	***D*—H···*A***
C2—H2···Cl2^{i}	0.93	2.99	3.727 (3)	137
C5—H5*A*···Cl2^{ii}	0.96	2.74	3.542 (3)	141
C6—H6*A*···Cl2^{i}	0.96	2.86	3.711 (4)	148
C8—H8···Cl3^{iii}	0.93	2.84	3.611 (3)	141
C11—H11*A*···Cl3^{iii}	0.96	2.85	3.681 (5)	145
C12—H12*A*···Cl1^{ii}	0.96	2.83	3.776 (4)	168
N3—H3*A*···Cl4	0.86	2.41	3.248 (3)	165
N3—H3*B*···Cl1	0.86	2.45	3.268 (3)	160
N6—H6*D*···Cl2	0.86	2.53	3.261 (3)	144
N6—H6*E*···Cl3^{iv}	0.86	2.35	3.184 (3)	164

Symmetry codes: (i) −*x*, −*y*, −*z*+1; (ii) *x*−1, *y*, *z*; (iii) −*x*−1, −*y*, −*z*; (iv) −*x*−½, *y*+½, −*z*+½.

Within the organic ligands 2-amino-4,6-dimethoxypyrimidine, an examination of the bond lengths data (Table 2) shows that all the C_{cycle}-O distances (C1—O1 [1.328 (4) Å], C3—O2 [1.339 (4) Å], C7—O3 [1.330 (4)] and C9—O4 [1.324 (4)]) are shorter than the C-O

methoxy bond lengths (C5—O1 [1.430 (4) Å], C6—O2 [1.443 (4)], C11—O3 [1.442 (4)] and C12—O4 [1.449 (4)]). This can be attributed to the donor mesomeric effect of the methoxy group [33-35]. Furthermore, the C–N bond distances of the NH_2 groups ([C4—N3]= 1.327 (4) Å and [C10—N6]= 1.336 (4) Å) are short for C–N single bonds, but still not quite as contracted as one would expect for a fully established C=N double bond. These bond length features are consistent with an imino resonance form as it is commonly found for a C-N single bond involving sp^2 hybridized C and N atoms [36, 37].

Table 4. Analysis of contacts on the Hirshfeld surface. Reciprocal contacts X…Y and Y…X are merged. The second line shows the chemical content on the surface. The % of contact types between chemical species is given followed by their enrichment ratio. The major contacts as well as the major enriched ones are highlighted in bold characters. The hydrophobic hydrogen atoms bound to carbon (Hc) were distinguished from the more polar one bound to nitrogen (Hn).

atom	Zn	Cl	N	O	Hn	Hc	C
%	11.0	28.3	7.7	5.6	8.1	26.1	13.2
Zn	0.0						
Cl	**13.7**	2.1		%	surface		
N	**8.1**	0.3	0.0				
O	3.5	1.4	1.6	0.0			
Hn	1.7	**10.2**	0.0	0.1	0.2		
Hc	2.7	**21.4**	3.6	1.1	2.2	5.1	
C	0.9	6.8	0.4	1.9	0.8	6.6	3.5
Zn	0						
Cl	**1.55**	0.25			enrichment		
N	**3.7**	0.08	0				
O	**2.3**	0.49	2.41	0			
Hn	0.72	**2.3**	0.03	0.12	0.35		
Hc	0.36	**1.54**	1.08	0.48	0.59	0.9	
C	0.23	0.96	0.21	1.66	0.41	1.14	**2.4**

3.2. Hirshfeld contacts analysis

Analysis of intermolecular interactions using the Hirshfeld surface represents a tool to gain insight into the crystal packing. The Hirshfeld surface was computed with the MoProViewer software [38]. The fingerprint plots (**Fig. 5**) were obtained from software CrystalExplorer3.1 [39]. The contact enrichment ratio E_{xy} between chemical species X and Y is obtained by comparing the actual contacts *C*xy in the crystal with those computed as if all types of contacts had the same probability to form. The chemical nature of contacts and their enrichment in the crystal structure are shown in Table 4. To obtain an integral Hirshfeld surface around each moiety (Zn(II), chloride anion and organic ligands), a set of entities not in contact with each other were selected in the crystal packing (**Fig. 6**).

The major contact is constituted by the weak C-H…Cl^-; it is moderately enriched (E_{xy}=1.54) as Hc and Cl^- are the most abundant atoms on the Hirshfeld surface (C_{xy}=21.4%). The strong hydrogen bond Cl^-…H-N is the second most abundant contact and is quite over-represented at E_{xy}=2.33. The zinc cation is interacting with Cl^-, N and O atoms and all these contacts are enriched, the Zn(II)…Cl^- ionic bridge being the most abundant and the Zn(II)…N the most enriched at *E*=3.7. The Cl^- anions are mostly interacting with the zinc cations and hydrogen atoms. The zinc cation is not coordinated by the methoxy oxygen atoms but there are four long distance attractive electrostatic interactions (in the 2.76-2.84 Å range) between these weakly polar oxygen atoms and the Zn(II) atom.

The self-contacts between charged species (Zn(II), $N^{\delta-}$, $O^{\delta-}$ and $Hn^{\delta+}$) are all strongly avoided with E_{xx} values equal or close to zero, as they represent electrostatic repulsion. The contact proportions C_{xy} of the two independent but identical organic ligands are very similar as they are 94.3% correlated.

40% of the surface is occupied by the hydrophobic Hc and C atoms and the C…C contacts are the most enriched at E_{xy} = 2.8. There is no parallel aromatic stacking occurring, rather the two cycles form contacts with the angle between the two planes being 78.6°. Slightly enriched C-H…π weak hydrogen bonds occur with the methyl groups. Globally the contacts between hydrophobic atoms are slightly enriched at E_{xy} = 1.17, those between polar atoms are normally represented (E_{xy}=0.99) while polar…hydrophobic interactions are only slightly impoverished (*E*=0.88) due to the presence of CH_3…Cl^- weak hydrogen bonds.

The electrostatic complementarity of molecules in a crystal packing can be mapped on the Hirshfeld surfaces [40]. The electrostatic potential (ESP) values on the Hirshfeld surface around the two independent organic ligands are shown in **Fig. 7**. The ESP was computed using software MoPro [41] using a multipolar atom model transferred from the ELMAM2 electron density database [42]. Electroneutrality constraint was applied after transfer to the asymmetric unit by adjusting the charge of Zn cation to +1.2e, while the transferred charge of Cl^- was -0.56e.

The inner and outer ESP values are anticorrelated with r=-0.57 and -0.65 for the ligand #1 and #2, respectively. In both cases, the outer potential shows mostly electropositive values on the surface while the inner potential shows more balanced positive and negative values. This is due to the fact that the ligand was modeled with a global negative charge of -0.08e while the "external" $ZnCl_2$ moiety bears a charge of +0.08e. The two ligands have in common the strong $N^{\delta-}$…Zn(II) coordination contacts with strong negative/inner and positive/outer ESP values. The strong Hn…Cl^- hydrogen bonds are also shared by the two ligands with highly positive inner ESP values. The negative outer ESP around the chloride anions is attenuated by the nearby presence of Zn(II) cation. Significant Hc…Cl^- weak H-bonds are also visible for both ligands in **Fig. 7a,b** in regions of weaker inner ESP. The O…Zn contacts occur for the two ligands and involves the most negative inner ESP values. Globally, the two scatterplots show very similar trends for the two independent molecules.

3.3. NMR results

The ^{13}C CP–MAS NMR spectrum of the coordination polymer $[Zn_2Cl_4(C_6H_9N_3O_2)_2]_n$ is shown in **Fig. 8**. It exhibits in the resonance domain of the methoxy groups, between 57.9 and 60.6 ppm, three sharp resonances with one of the peaks, at 57.9 ppm, having about double the integrated intensity of the other two and corresponding to the four crystallographically independent methoxy carbon atoms, . The spectrum can thus be interpreted as featuring four resonances in this region, with two of them in close proximity with substantial overlap. This is in agreement with two organic molecules being present in the asymmetric unit cell as revealed by X-ray structure determination. The peak at 78.6 ppm corresponds to the C5 carbon atom since it is located between two carbon atoms of the pyrimidine ring, so it is the most shielded (see below for the calculation of the NMR chemical shifts). The carbon atoms C4 and C6, which are linked to oxygen, have practically the same chemical environment and therefore they are the less shielded and resonate at 172.8 ppm.

The ^{15}N CP-MAS NMR spectrum of the title compound, presented in **Fig. 9**, exhibits two well-resolved peaks. The first one at -287.5 ppm is assigned to aliphatic nitrogen atoms of the NH_2 groups, while the second one, at -211.7 ppm, corresponds to the aromatic nitrogen atoms.

Theoretical calculations were undertaken in order to assign the NMR resonances to the different crystallographic non-equivalent carbon and nitrogen atoms of the unit cell. All calculations were carried out with Gaussian 09, the B3LYP method and the 6-31+G * base for all atoms. In a first study, the calculations were made on a system containing only one zinc complex with its two surrounding organic ligands but as one nitrogen of the organic molecule is also linked to another metallic atom, these calculations cannot allow a good determination of the chemical displacements in NMR and therefore another calculations were carried out by adding two $ZnCl_2$ groups and completing the coordination around these two zinc atoms with an NH_3 group. In both cases the positions of the protons were optimized before doing these calculations. The atoms are labeled as depicted below:

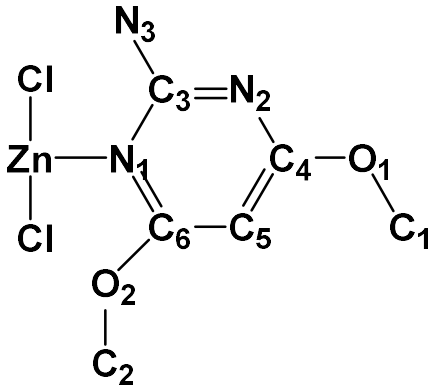

The results are listed in **Table 5**. Clearly, there is a very good agreement between the experimental and theoretical values calculated after optimization of the position of the protons, allowing unambiguously the attribution of the different NMR signals.

Table 5. Comparison of calculated and experimental chemical shift values (ppm) of carbon and nitrogen atoms in the title complex.

Atoms	Complex		Complex + 2 $ZnCl_2(NH_3)$		Experiment
C1	53.5	55.2	52.6	54.7	57.9
C2	54.1	54.0	54.9	55.0	59.6 and 60.5
C3	154.2	154.5	152.0	152.7	159.6

C4	165.9	165.2	163.4	163.1	172.8
C5	63.9	63.2	64.1	63.8	78.2
C6	162.6	161.9	165.0	165.2	172.8
N1	-192.4	-189.2	-192.8	-188.2	-211.7
N2	-149.5	-155.1	-191.6	-195.6	-211.7
N3	-277.0	-273.7	-258.4	-254.1	-287.5

3.4. Quantum mechanical study

DFT calculations were made (by use of the B3LYP/6-31+G* method for all atoms) on the geometry obtained after optimization of the protons. The energies of the frontier orbitals in the two calculation models are listed in **Table 6**. It follows from these calculations that the HOMO is localized essentially on the chlorine atoms, whatever the chosen model, while the LUMO is localized on the organic groups (**Figs. 10a** and **10b**). The difference in HOMO / LUMO energy is 5.46 eV in the case of the complex alone and 4.34 eV if the $ZnCl_2NH_3$ groups are added, values proving the stability of this compound. The energy distribution of the different orbitals for both cases (**Fig. 11)** shows a great analogy between the two distributions.

Table 6. Energy values of frontier orbitals (eV) in the title complex.

Energy (eV) / Orbitals	Zn complex alone	Zn complex + 2 $ZnCl_2NH_3$ groups
HOMO-5		-7.13
HOMO-4		-7.10
HOMO-3		-6.90
HOMO-2		-6.86
HOMO-1		-6.66
HOMO	**-6.53**	**-6.65**
LUMO	**-1.07**	**-2.31**
LUMO+1		-2.23
LUMO+2		-1.50

3.5. Molecular Electrostatic Potential analysis (MEP)

The Molecular Electrostatic Potential (MEP) surface is depicted on **Fig. 12**. The MEP is used to determine the nuclear and electronic charge distribution of a given molecule. The maps were obtained at the B3LYP/6-31+G* level of theory. As it can be seen, the electrostatic potential maps are color-coded and are subdivided into many regions where those various colors are used to identify different potentials. Blue and red colors indicate the positive and negative potentials, respectively. In both cases, the most negative zones are on the aromatic ring, while the most positive ones are located at the protons bonded to the nitrogen atom.

3.6. IR spectroscopy

FT-IR spectroscopy was used to verify the functional groups present in the crystal, and to investigate their vibrational behavior in the solid state. The IR spectrum of $[Zn_2Cl_4(C_6H_9N_3O_2)_2]_n$ is shown in **Fig. 13a**. The assignments of the observed bands are based on comparisons with data previously reported for similar materials [43-45]. The bands in the high-wavenumber region, between 3500 and 3200 cm^{-1}, correspond to the stretching vibrations of the N-H and O-H groups interconnected by a system of hydrogen bonds in the crystal [44]. The weak band at 2942 cm^{-1} corresponds to the C-H stretching modes. The bands at 1667 and 1607 cm^{-1} are assigned to the stretching vibrations of C=C and C=N groups and to the N-H bending vibration modes [46, 47]. The bands of medium intensities observed at 1470 and 1385 cm^{-1} are associated to the C–H asymmetric and symmetric bending vibrations, respectively. The characteristic absorption peak at 1223 cm^{-1} can be associated to Ar-O-C stretching vibration. The observed bands in the 1200 -1000 cm^{-1} region correspond to the valence vibrations of C-C and C-N groups [48, 49]. The bands in the range 1000–600 cm^{-1} can be attributed to the out of plane bending modes of C-H, N-H, C-C and C-N groups [50]. DFT calculations of the frequencies were made by use of the B3LYP/6-31+G* method on the geometry obtained after optimization of the protons. The resulting IR spectrum between 4000 and 400 cm^{-1} is shown on **Fig. 13-b** and is very similar to the experimental one. A close agreement between the experimental and theoretical wave numbers ($R^2 = 0.9932$) is mostly achieved in the finger print region as shown in **Fig. 14**. Thus, the precision is well-sufficient to assign the experimental frequencies and to confirm the attributions proposed above.

4. Conclusions

A new Zn(II) polymeric complex with the 2-amino-4,6-dimethoxypyrimidine, $[Zn_2Cl_4(C_6H_9N_3O_2)_2]_n$, has been prepared at room temperature. In the title compound, the organic entity behaves as a neutral bidentate ligand and Zn(II) adopts a tetrahedral coordination. The contacts enrichment ratios derived from the Hirshfeld surface analysis shows that besides formation of the Zn(II) metal coordination complex with N ligands and chloride anions, the crystal packing is mainly stabilized by N/C-H…O and N/C-H…Cl^- hydrogen bonds. The MEP map defines the nucleophile and the electrophile sites. The band gap energy between HOMO and LUMO indicates that the title compound is kinetically stable. NMR signals are in full agreement with the crystallographic data. DFT calculations allow the attribution of the experimental NMR lines and of IR bands at low frequencies. As a solution study has not been done, we cannot know if this complex is stable in solution.

Supplementary data

Crystallographic data for the structural analysis have been deposited at the Cambridge Crystallographic Data Centre, CCDC No 1983914. These data can be obtained free of charge via http://www.ccdc.cam.ac.uk/conts/retrieving.html, or from the CCDC, 12 Union Road, Cambridge, CB2 1EZ, UK: fax: (+44) 01223-336-033; e-mail: deposit@ccdc.cam.ac.

References

[1] V.C. Gibson, C. Redshaw, G.A. Solan, Chem. Rev. 107 (2007) 1745-1776.

[2] M. Białek, A. Białon´ ska, L. Latos-Gra_zyn´ ski, Inorg. Chem. 54 (2015) 6184-6194.

[3] (a) K. Sumida, D.L. Rogow, J.A. Mason, T.M. McDonald, E.D. Bloch, Z.R. Herm, T.H. Bae, J.R. Long, Chem. Rev. 112 (2012) 724–781;

(b) R.B. Getman, Y.-S. Bae, C.E. Wilmer, R.Q. Snurr, Chem. Rev. 112 (2012) 703–723;

(c) H. Wu, Q. Gong, D.H. Olson, J. Li, Chem. Rev. 112 (2012) 836–868.

[4] (a) J.-R. Li, J. Sculley, H.-C. Zhou, Chem. Rev. 112 (2012) 869–932;

(b) B.V. Voorde, B. Bueken, J. Denayerb, D.D. Vos, Chem. Soc. Rev. 43 (2014) 5766-5788.

[5] (a) S. Goswami, H. S. Jena, S. Konar, Inorg. Chem. 53 (2014) 7071−7073

(b) C.K. Brozek, M. Dincă, Chem. Soc. Rev. 43 (2014) 5456–5467;

(c) B. Manna, S. Singh, A. Karmakar, A.V. Desai, S.K. Ghosh, Inorg. Chem. 54 (2015) 110–116.

[6] (a) A. Corma, H. Garcia, F.X.L. Xamena, Chem. Rev. 110 (2010) 4606–4655;

(b) M. Yoon, R. Srirambalaji, K. Kim, Chem. Rev. 112 (2012) 1196–1231;

(c) J. Liu, L. Chen, H. Cui, J. Zhang, L. Zhang, C.-Y. Su, Chem. Soc. Rev. 43 (2014) 6011–6061.

[7] (a) P. Dechambenoit, J.R. Long, Chem. Soc. Rev. 40 (2011) 3249–3265;

(b) E. Coronado, G.M. Espallargas, Chem. Soc. Rev. 42 (2013) 1525–1539.

(c) W.-X. Zhang, P.-Q. Liao, R.-B. Lin, Y.-S. Wei, M.-H. Zeng, X.-M. Chen, Coord. Chem. Rev. 293 (2015) 263–278.

(d) X.-S. Gao, H.-J. Dai, Y. Tang, M.-J. Ding, W.-B. Pei, X.-M. Ren, ACS Omega 4 (2019) 12230−12237.

(e) H. Meng, C. Zhao, M. Nie, C. Wang**,** T. Wang, ACS Appl. Mater. Interfaces 10 (2018) 32607-32612

[8] (a) S. Khatua, S. Goswami, S. Biswas, K. Tomar, H. S. Jena, S. Konar, Chem. Mater. 27 (2015) 5349-5360;

(b) L.E. Kreno, K. Leong, O.K. Farha, M. Allendorf, R.P. Van Duyne, J.T. Hupp, Chem. Rev. 112 (2012) 1105–1125;

(c) Y. Cui, Y. Yue, G. Qian, B. Chen, Chem. Rev. 112 (2012) 1126–1162;

(d) Z. Hu, B.J. Deibert, J. Li, Chem. Soc. Rev. 43 (2014) 5815–5840.

[9] B. Konig, M. Pelka, H. Zieg, P. G. Jones, I. Dix, Chem. Commun. (1996) 471–472.

[10] T. J. Norman, D. Parker, F. C. Smith, D. J. King, J. Chem. Soc. Chem. Commun. (1995) 1879–1880.

[11] M. Afzal, C.L. Rosenberg, M.A. Malik, A.J.P. White, P. O'Brien, New J. Chem. 35 (2011) 2773–2780.

[12] I. Haiduc, R. Cea-Olivares, R.A. Toscano, C. Silvestru, Polyhedron 14 (1995) 1067-1071.

[13] L.M. Nguyen, M.E. Dellinger, J.T. Lee, R.A. Quinlan, A.L. Rheingold, R.D. Pike, Inorg. Chim. Acta 358 (2005) 1331-1336.

[14] D.G. Cutell, S. Kuang, P.E. Fanwick, D.R. McMillin, R.A. Walton, J. Am. Chem. Soc. 124 (2002) 6-7.

[15] S. Kuang, D.G. Cutell, D.R. McMillin, P.E. Fanwick, R.A. Walton, Inorg. Chem. 41 (2002) 3313-3322.

[16] P. Aslanidis, P.J. Cox, S. Divanidis, A.C. Tsipis, Inorg. Chem. 41 (2002) 6875-6886.

[17] H. Xu, Z. Chen, S. Ishizaka, N. Kitamura, J. Wu, Chem. Commun. (2002) 1934-1935.

[18] (a) P.K. Pal, S. Mohapatra, A.D. Jana, G.K. Patra, J. Mol. Struct. 1015 (2012) 156-161,

(b) M.A. Braverman, R.M. Supkowski, R.L. LaDuca, J. Solid State Chem. 180 (2007) 1852-1862,

(c) S.M. Vickers, P.D. Frischmann, M.J. MacLachlan, Inorg. Chem. 50 (2011) 2957-2965;

(d) S. Ray, S. Konar, A. Jana, S. Jana, A. Patra, S. Chatterjee, J.A. Golen, A.L. Rheingold, S.S. Mandal, S.K. Kar, Polyhedron 33 (2012) 82-89.

[19] S. Gupta, S. Pal, A.K. Barik, A. Hazra, S. Roy, T.N. Mandal, S.M. Peng, G.H. Lee, M.S.E. Fallah, J. Tercero, S.K. Kar, Polyhedron 27 (2008) 2519–2528.

[20] M.B. Bushuev, K.A. Vinogradova, V.P. Krivopalov, E.B. Nikolaenkova, N.V. Pervukhina, D.Y. Naumov, M.I. Rakhmanova, E.M. Uskov, L.A. Sheludyakova, A.V. Alekseev, S.V. Larionov, Inorg. Chim. Acta 371 (2011) 88–94.

[21] A.B. Caballero, A. Rodriguez-Dieguez, E. Barea, M. Quiros, J.M. Salas, Cryst. Eng. Commun. 12 (2010) 3038–3045.

[22] M. Wojtaś, A. Gągor, O. Czupiński, A. Piecha-Bisiorek, D. Isakov, W. Medycki, R. Jakubas, CrystEngComm 17 (2015) 3171–3180.

[23] Z. Otwinowsky, W. Minor, In: Methods in Enzymology; C. W. Carter, R. M. Jr. Sweet, (Eds.); Academic Press: New York, 1997, 276, 307-326.

[24] (a) A. Altomare, C. Burla, M. Camalli, L. Cascarano, C. Giacovazzo, A. Guagliardi, A.G.G. Moliterni, G. Polidori, R. Spagna, J. Appl. Cryst. 32 (1999,) 115-119;

(b) A. Altomare, G. Cascarano, C. Giacovazzo, A. Guagliardi, J. Appl. Cryst. 26 (1993) 343-350.

[25] G. M. Sheldrick, SHELXL-97, University of Gottingen, Germany 1997.

[26] S. Mackay, C. Edwards, A. Henderson, C. Gilmore, N. Stewart, K. Shankland, A. Donald, University of Glasgow, Scotland 1997.

[27] D. Waasmaier, A. Kirfel, Acta Crystallogr. A 51 **(**1995) 416-431

[28] K. Brandenburg, Diamond Version 2.0 Impact GbR, Bonn., Germany (1998)

[29] M. J. Frisch, G.W. Trucks, H.B. Schlegel, G.E. Scuseria, M.A. Robb, J.R. Cheeseman, G. Scalmani, V. Barone, B. Mennucci, G.A. Petersson, H. Nakatsuji, M. Caricato, X. Li, H.P. Hratchian, A.F. Izmaylov, J. Bloino, G. Zheng, J.L. Sonnenberg, M. Hada, M. Ehara, K. Toyota, R. Fukuda, J. Hasegawa, M. Ishida, T. Nakajima, Y. Honda, O. Kitao, H. Nakai, T. Vreven, J.A. Montgomery Jr., J.E. Peralta, F. Ogliaro, M. Bearpark, J.J. Heyd, E. Brothers, K.N. Kudin, V.N. Staroverov, T. Keith, R. Kobayashi, J. Normand,

K. Raghavachari, A. Rendell, J.C. Burant, S.S. Iyengar, J. Tomasi, M. Cossi, N. Rega, J.M. Millam, M. Klene, J.E. Knox, J.B. Cross, V. Bakken, C. Adamo, J. Jaramillo, R. Gomperts, R.E. Stratmann, O. Yazyev, A.J. Austin, R. Cammi, C. Pomelli, J.W. Ochterski, R.L. Martin, K. Morokuma, V.G. Zakrzewski, G.A. Voth, P. Salvador, J.J. Dannenberg, S. Dapprich, A.D. Daniels, O. Farkas, J.B. Foresman, J.V. Ortiz, J. Cioslowski, D.J. Fox, Gaussian 09, Revision B.01, Gaussian, Inc., Wallingford CT, 2010

[30] W. Nbili, M. Zeller, F. Lefebvre, C. Ben Nasr, J. Mol. Struct. 1085 (2015) 37-44

[31] M. B. Bushuev, K. A. Vinogradova, V. P. Krivopalov, E. B. Nikolaenkova, N. V. Pervukhina, D. Y. Naumov, M. I. Rakhmanova, E. M. Uskov, L. A. Sheludyakova, A. V. Alekseev, S. V. Larionov, Inorg. Chim. Acta 371 (2011) 88-94.

[32] L. Yang, D. R. Powell, R. P. Houser, Dalton Trans. 9 (2007) 955-64.

[33] P.R. Lowe, C.H. Schwalbe, G.J.B. Williams, ActaCryst. C 43 (1987) 330-333.

[34] L.M. Toledo, K. Musa, J.W. Lauher, F.W. Fowler, Chem. Mater. 7 (1995) 1639-1647.

[35] V. Gerhardt, M. Tutughamiarso, M. Bolte, ActaCryst. C 67 (2011) 179-187.

[36] R. N. Yang, D. M. Wang, Y. M. Hou, B. Y. Xue, D. M. Jin, L. R. Chen, B. S. Luo, Acta Chem. Scand. 49 (1995) 771-773.

[37] R. Grobelny, T. Glowiak, J. Mrozinski, W. Baran, P. Tomasik, Pol. J. Chem. 69 (1995) 559-565.

[38] B. Guillot, E. Enrique, L. Huder, C. Jelsch, Acta Cryst. A70 (2014) C279

[39] J. J. McKinnon, D. Jayatilaka, M. A. Spackman, 37 (2007) 3814-3816.

[40] M. A. Spackman, J. J. McKinnon, D. Jayatilaka, CrystEngComm, 10 (2008). 377-388.

[41] C. Jelsch, S. Soudani, C. Ben Nasr, IUCrJ 2 (2015) 327-340.

[42] S. Domagała, B. Fournier, D. Liebschner, B. Guillot, C. Jelsch, Acta Crys. A 68 (2012) 337-351.

[43] K. Klai, C. Jelsch , F. Lefebvre, V. Ferretti, C. Ben Nasr, K. Kaabi, Solid State Sci. 101 (2020) 106-119.

[44] W. Nbili, S. Soudani, K. Kaabi, M. Wojtaś, V. Ferretti, F. Lefebvre, C. Jelsche, C .Ben Nasr, J. Mol. Struct. 1146 (2017) 347-355.

[45] W. Nbili, K. Kaabi, F. Lefebvre, W. Kaminsky, C. Ben Nasr, Chem. Data Coll. 17 (2018) 345–355.

[46] S. Soudani, E. Jeanneau, C. Jelsch, F. Lefebvre, C. Ben Nasr, J. Mol. Struct. 1123 (2016) 66–74.

[47] S. Belhaj Salah, P. S. Pereira da Silva, F. Lefebvre, C. Ben Nasr, S. Ammar, M. L. Mrad, J. Mol. Struct. 1137 (2017) 553–561.

[48] Z. Aloui, V. Ferretti, S. Abid, M. Rzaigui, F. Lefebvre, C. Ben Nasr, J. Mol. Struct. 1087 (2015) 26–32.

[49] C. Bjeoui, I. Ameur, N. Derbel, A. Linden, S. Abid, J. Mol. Struct. 1166 (2018) 7–14.

[50] M. L. Mrad, I. Feddaoui, M. S. M. Abdelbaky, S. Garcia-granda, C. Ben Nasr, Inorg. Chim. Acta. 476 (2018) 38–45.

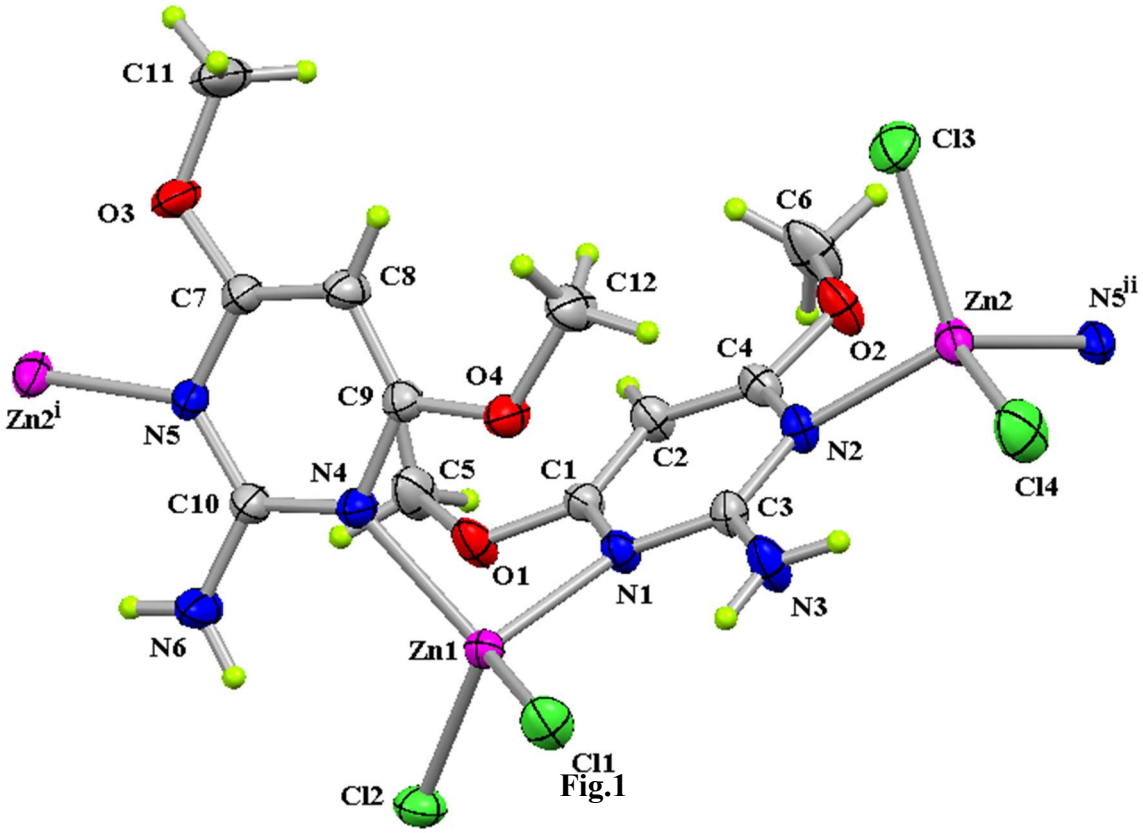

Fig.1

Molecular structure of the polymeric complex $[Zn_2Cl_4(C_6H_9N_3O_2)_2]_n$ with thermal displacement ellipsoids drawn at the 40% probability level. Symmetry codes: i = -½ – x, ½ + y, ½ - z, ii = -½ – x, -½

+ y, ½ – z.

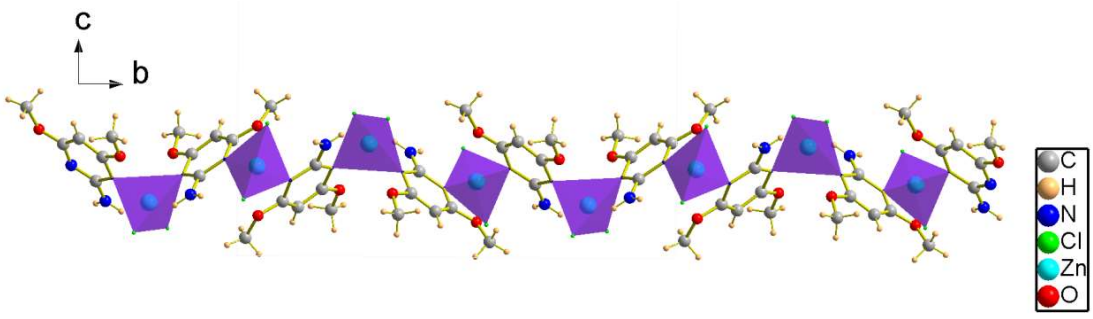

Fig. 2

View of 1D zigzag chain $[Zn_2Cl_4(C_6H_9N_3O_2)_2]_n$ along the *a*-axis.

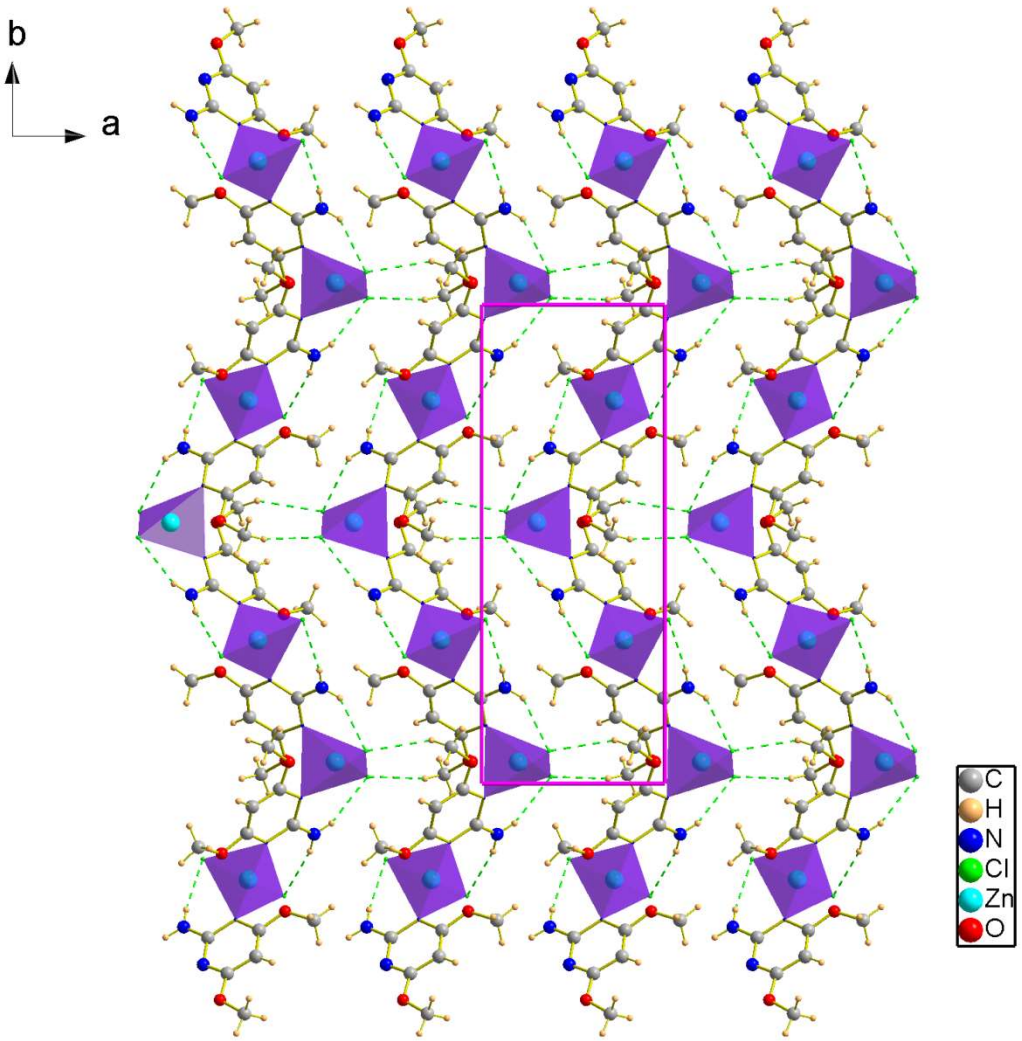

Fig. 3

Projection along the *c*-axis direction of a layer of the coordination polymer $[Zn_2Cl_4(C_6H_9N_3O_2)_2]_n$. Dotted lines indicate hydrogen bonds.

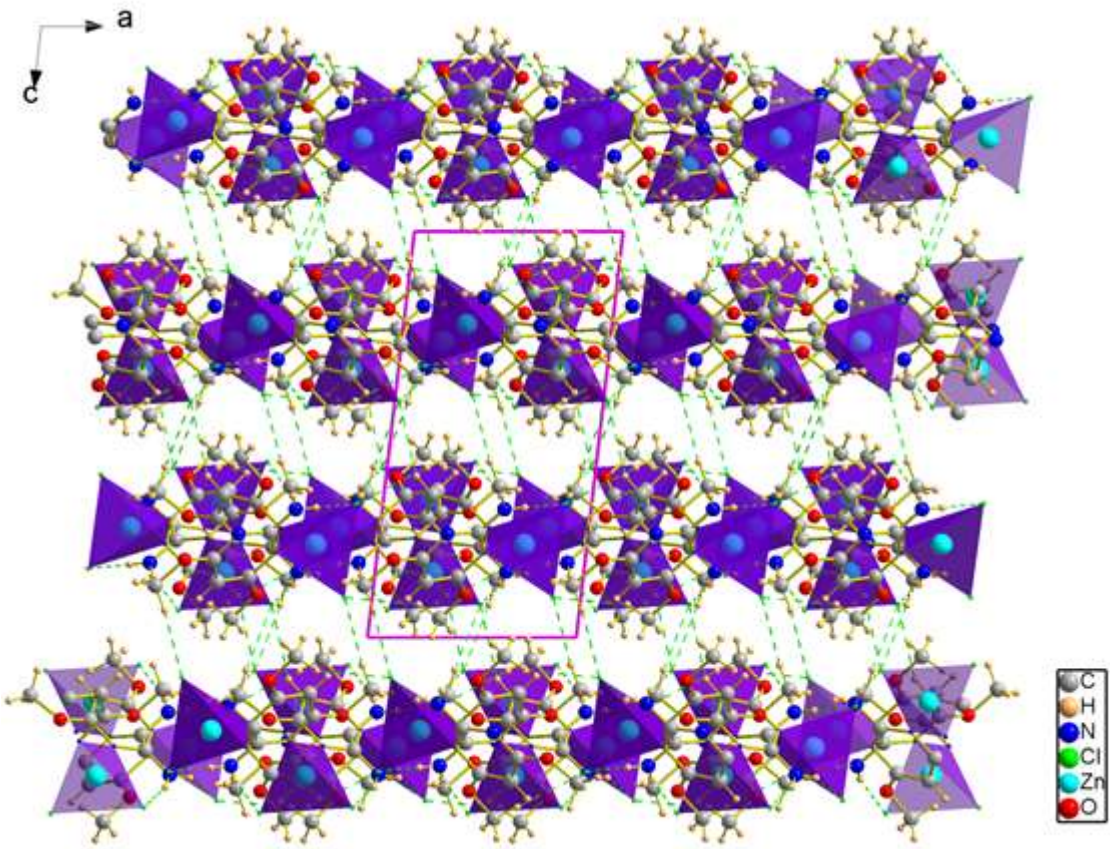

Fig. 4

A projection of the structure of the coordination polymer $[Zn_2Cl_4(C_6H_9N_3O_2)_2]_n$ along the *b*-axis. Dotted lines indicate hydrogen bonds.

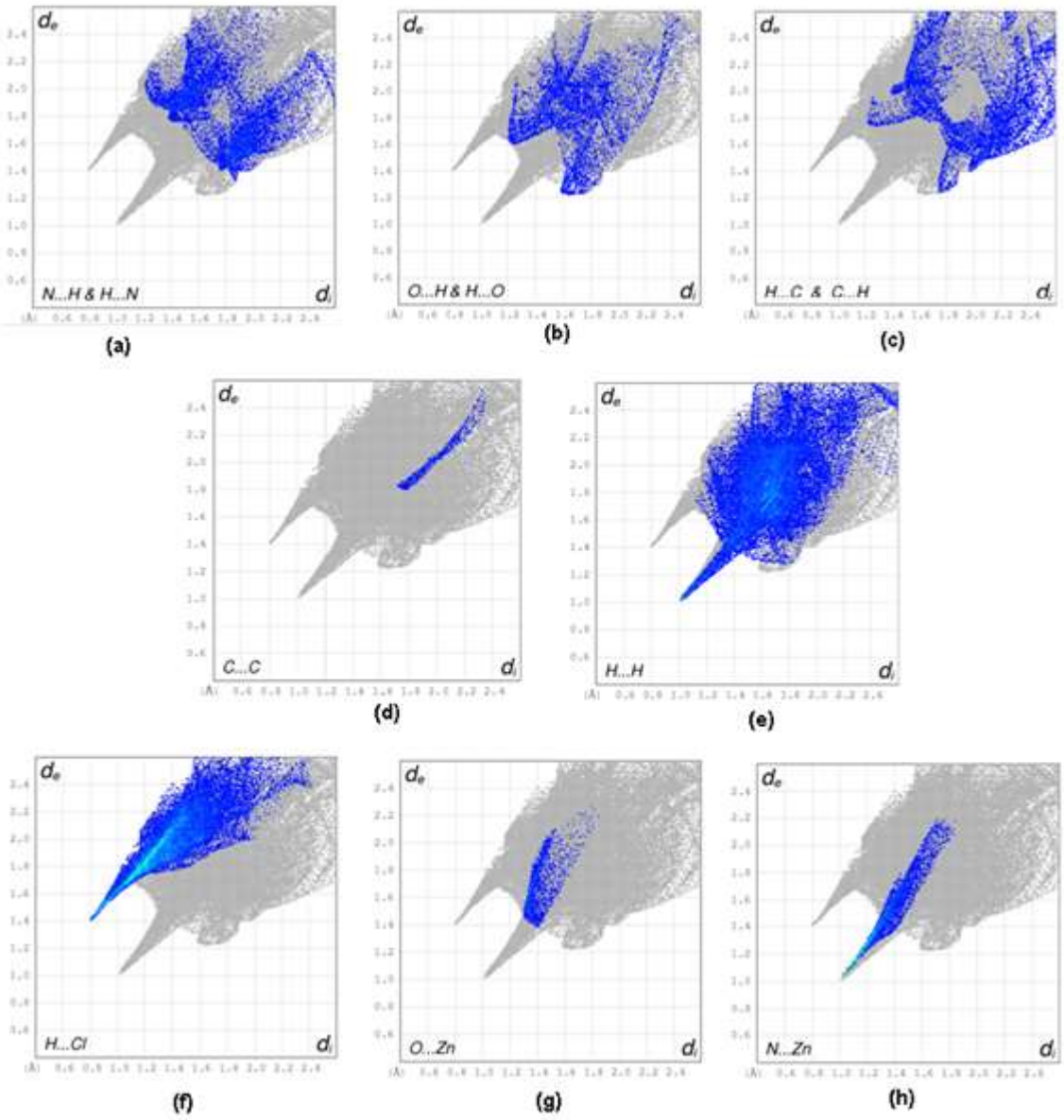

Fig. 5

Fingerprint plots of the main interactions in the crystal packing.

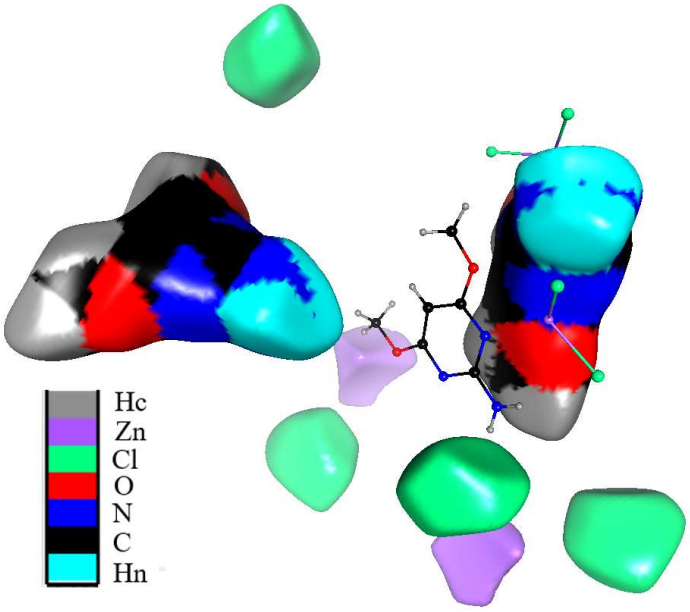

(a)

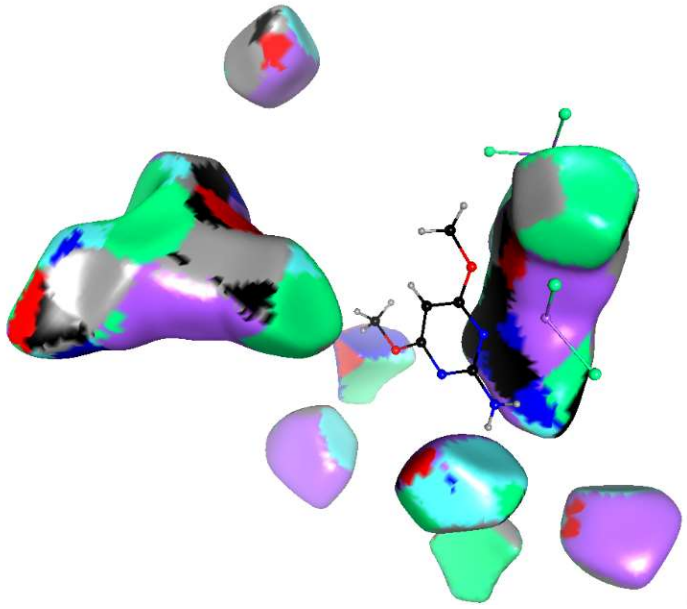

(b)

Fig. 6

View of the Hirshfeld surface around all the moieties of the title compound coloured according to the atoms in contact. (a) interior atom (b) exterior atom. The atoms and organic molecule surface on the top right represent the asymmetric unit.

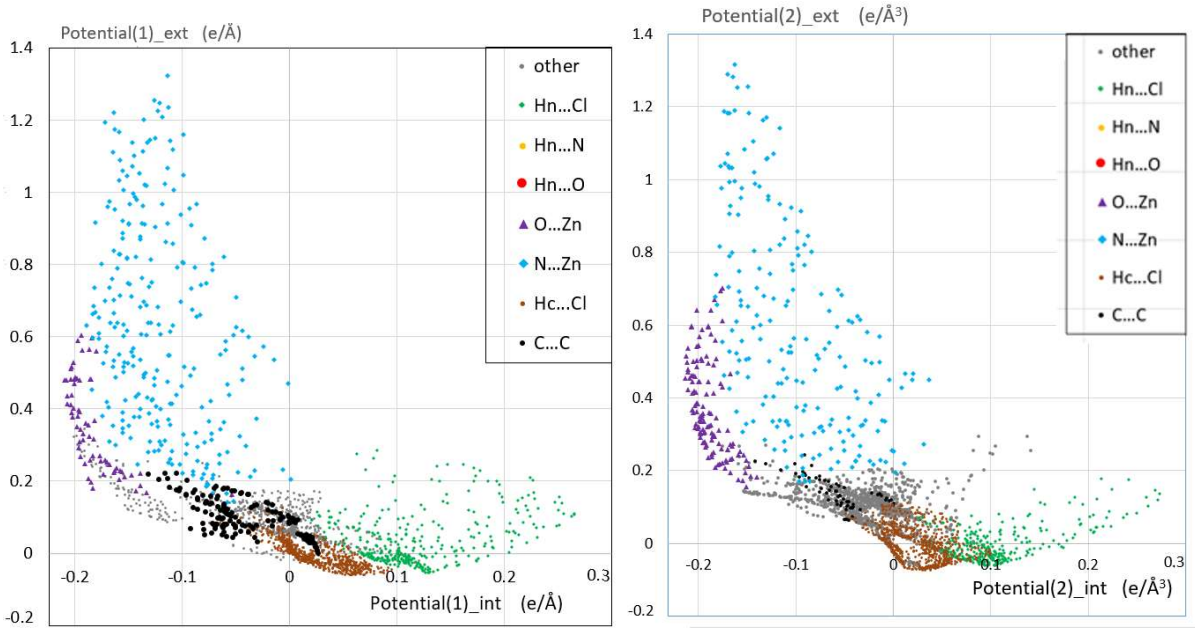

Fig. 7

Scatterplot of inner and outer electrostatic potential on the Hirshfeld surface of the two independent 2-amino-4,6-dimethoxypyrimidine ligands (molecule #1 bears atom N1). The inner ESP is obtained from the molecule alone. The outer ESP is generated by the rest of the asymmetric unit (AU) content and the surrounding symmetry related AUs which are in contact with the molecule. The main and strongest interactions are colored according to the chemical atom types.

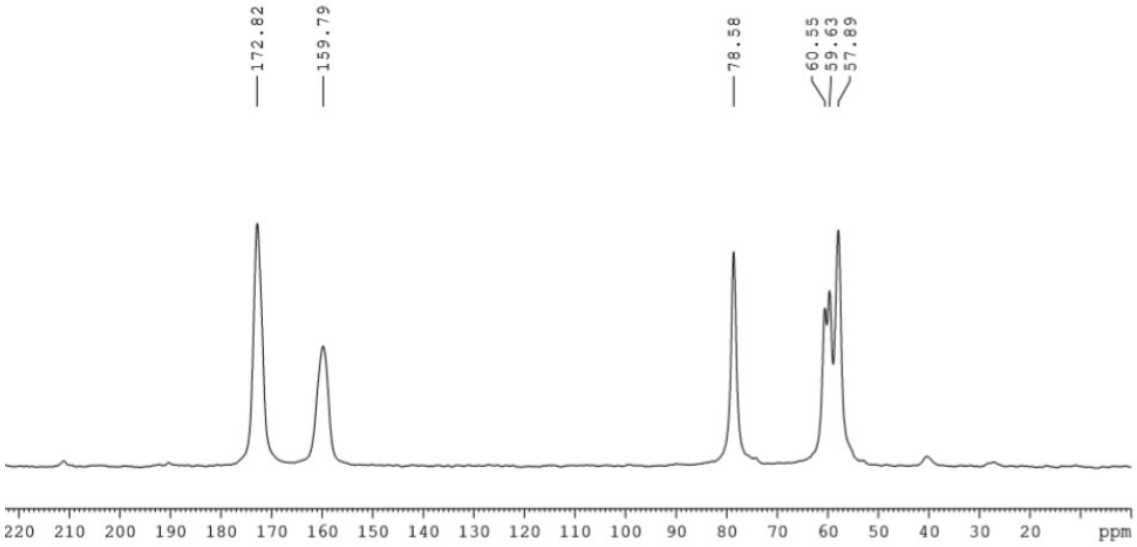

Fig. 8 ^{13}C CP-MAS NMR spectrum of the polymeric complex $[Zn_2Cl_4(C_6H_9N_3O_2)_2]_n$

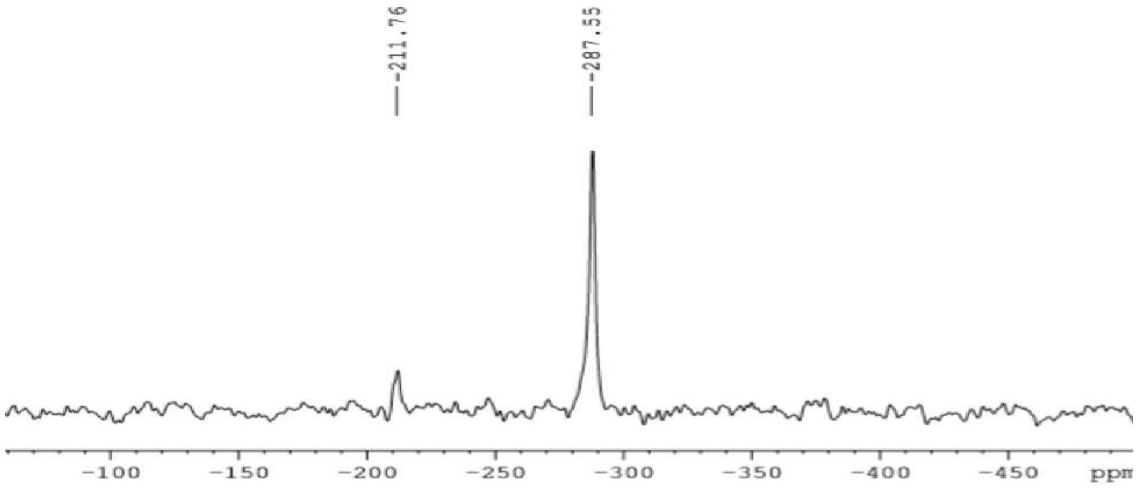

. **Fig. 9** ^{15}N CP-MAS NMR spectrum of the polymeric complex $[Zn_2Cl_4(C_6H_9N_3O_2)_2]_n$

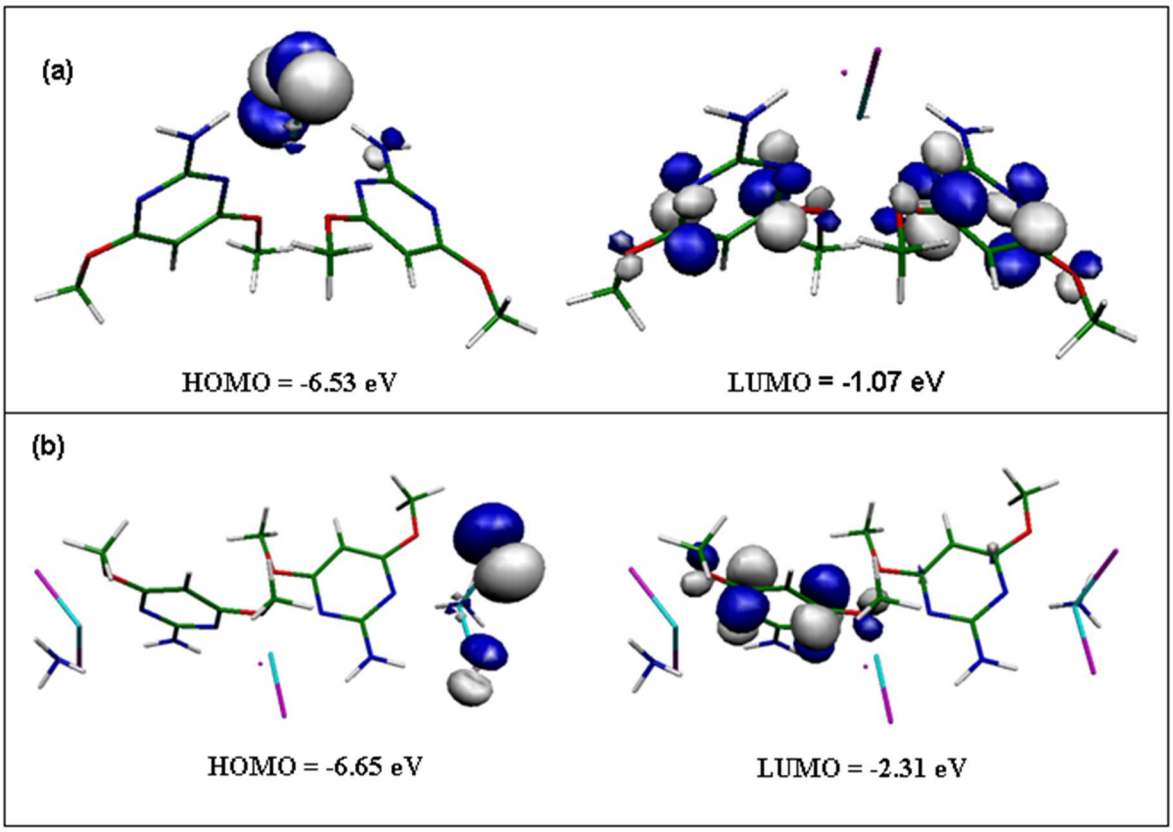

.**Fig. 10** Frontier orbitals in the polymeric complex $[Zn_2Cl_4(C_6H_9N_3O_2)_2]_n$.
(a) With only a zinc complex. (b) With adding two $ZnCl_2$ and two NH_3 groups.

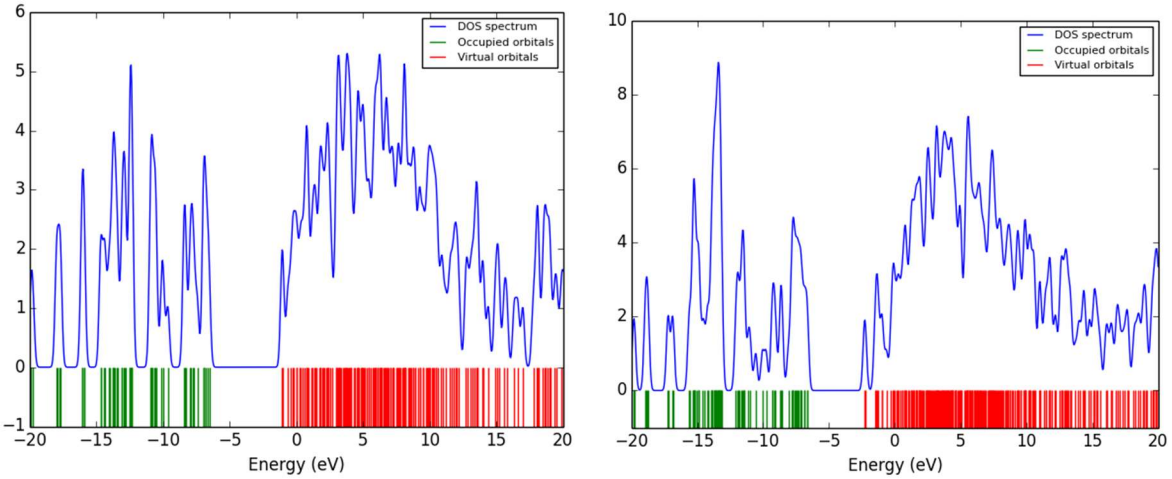

Fig. 11 Energy distribution of the different orbitals for the polymeric complex $[Zn_2Cl_4(C_6H_9N_3O_2)_2]_n$. With only a zinc complex (left). With adding two $ZnCl_2$ and two NH_3 groups (right).

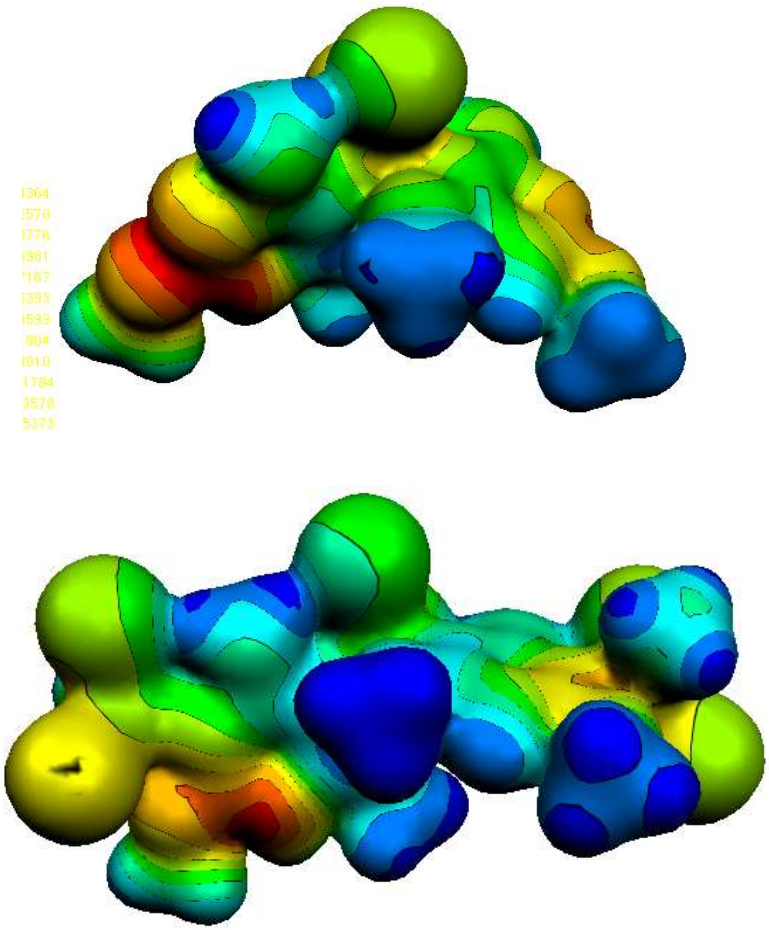

Fig. 12

MEP surface of the polymeric complex $[Zn_2Cl_4(C_6H_9N_3O_2)_2]_n$.

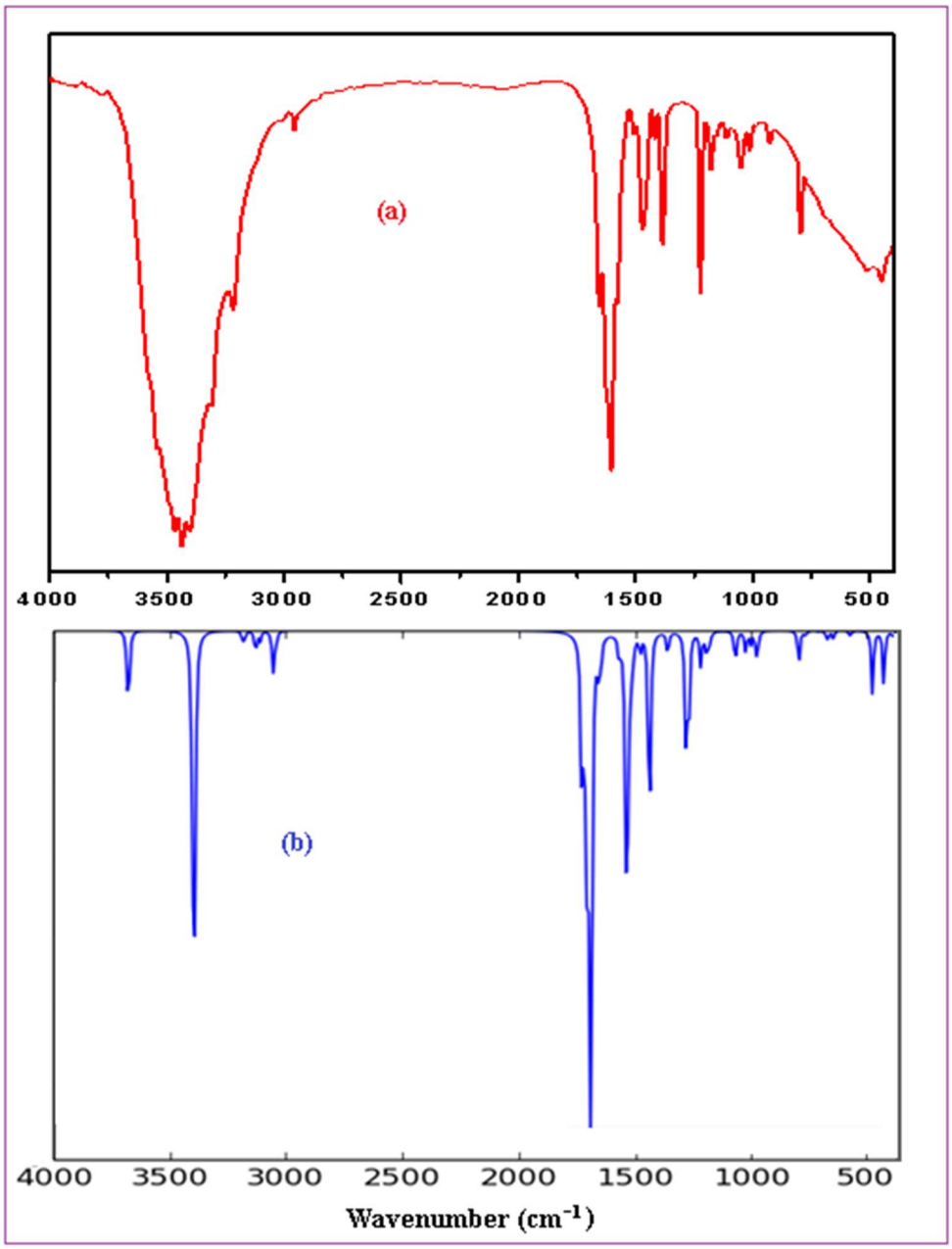

Fig. 13

(a) Experimental and (b) Calculated infrared absorption spectrum of the polymeric complex $[Zn_2Cl_4(C_6H_9N_3O_2)_2]_n$.

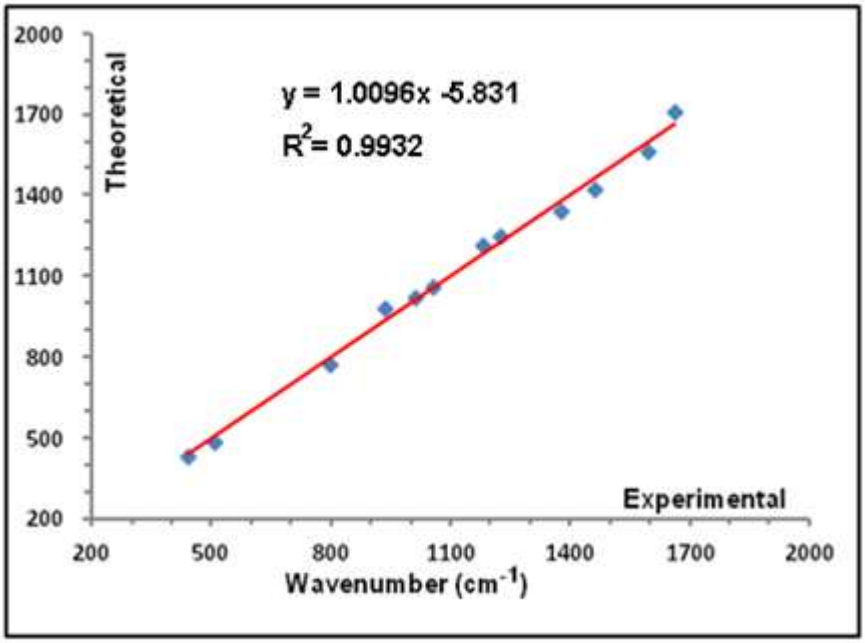

Fig. 14

Comparison between experimental and calculated IR frequencies of the polymeric complex $[Zn_2Cl_4(C_6H_9N_3O_2)_2]_n$.